NON-COHERENT MODULATION WITH RANDOM PHASE CONFIGURATIONS IN RIS-EMPOWERED CELLULAR MIMO SYSTEMS

Kun Chen-Hu[1], G. C. Alexandropoulos[2], Ana Garcia Armada[1]
[1]Department of Signal Theory and Communications of Universidad Carlos III of Madrid, 28911, Leganés, Spain. E-mails: {kchen, agarcia}@tsc.uc3m.es, [2]Department of Informatics and Telecommunications, National and Kapodistrian University of Athens, 15784 Athens, Greece. E-mail: alexandg@di.uoa.gr.

NOTE: Corresponding author: Kun Chen-Hu, kchen@tsc.uc3m.es

Abstract *– The Reconfigurable Intelligent Surface (RIS) constitutes one of the prominent technologies for the 6th Generation (6G) of wireless communications. It is envisioned to enhance signal coverage in cases where obstacles block direct communication from Base Stations (BSs), and when high carrier frequencies are used that are sensitive to attenuation losses. In the literature, the exploitation of RISs based on traditional coherent demodulation, relies on the availability of accurate Channel State Information (CSI). Given that CSI estimation, a multi-antenna BS or a dedicated orchestration controller jointly computes the pre-coder/combiner and the RIS configuration. The latter tasks require a significant amount of time and resources, which may not be affordable when the channel is time-varying or the CSI is not accurate enough. In this paper, we consider the uplink between a single-antenna user and a multi-antenna BS, and present a novel RIS-empowered Orthogonal Frequency Division Multiplexing (OFDM) communication system, which is based on differential phase shift keying combined with random phase configurations at the RIS, thus, avoiding the channel estimation and any complex optimization processes. This feature renders our RIS-enabled system operation proposal suitable for high noise and/or mobility scenarios. Considering both an idealistic and a realistic channel model, analytical expressions for the Signal-to-Interference and Noise Ratio (SINR) and the Symbol Error Probability (SEP) of the proposed non-coherent RIS-empowered communication system are presented. Our extensive computer simulation results verify the accuracy of the presented analysis and showcase the proposed system's performance superiority over coherent demodulation in different mobility and spatial correlation scenarios.*

Keywords – Channel estimation, differential modulation, mobility, non-coherent system, random phase configuration, reconfigurable intelligent surface

1. INTRODUCTION

The evolving technology of Reconfigurable Intelligent Surfaces (RISs) [1, 2, 3, 4] is expected to play a significant role in the evolution of mobile communication systems, from the current 5th Generation (5G) [5] towards the 6th Generation (6G) [6]. The high frequency bands are already being extensively exploited for mobile communications [7], such as 3.5 GHz and millimeter waves, in order to take advantage of the huge available bandwidth and provide a fully enhanced Mobile Broadband (eMBB) experience. The Terahertz (THz) frequency band from 300 GHz to 3 THz, as defined by IEEE and ITU, is a strong candidate for ultra-high-rate 6G wireless applications [8]. However, the coverage in these bands will suffer from attenuation loss, and any obstacle may easily block the communication link. RIS-empowered links provide an appealing solution to both improve and extend the signal transmitted by either the Base Station (BS) or User Equipment (UE), without excessively increasing the overall cost of the wireless network.

RISs are lightweight and hardware-efficient artificial planar structures of almost passive reflective elements [4] that enable desired dynamic transformations of the signal propagation environment in wireless communications [2]. They can support a wide variety of electromagnetic functionalities [9], ranging from perfect and controllable absorption, beam and wavefront shaping to polarization control, broadband pulse delay, radio-coverage extension, and harmonic generation. The RIS technology is envisioned to coat objects in the wireless environment [2] (e.g., building facades and room walls), and can operate either as a reconfigurable reflector beyond Snell's law [1], or as an analog receiver [10] or lens [11] when equipped with a single Radio-Frequency (RF) chain, or as a transceiver with multiple relevant RF chains [12]; see the recent survey [13] with the up-to-date available RIS hardware architectures.

The exploitation of RISs is mainly based on the classical Coherent Demodulation Scheme (CDS) [14, 17, 18, 19, 20, 21, 22, 23, 24, 15, 16], where the knowledge of Channel State Information (CSI) is essential for the optimized configuration of the RIS tunable elements and the demodulation of the signal at the receiving node. An approach for estimating the cascaded channel matrix [18, 19, 16], which encompasses the joint effect of signal propagation over the BS-RIS and RIS-UE links, was proposed in [17]. Note that this channel cannot be easily decoupled with almost passive RISs that do not possess receive RF chains. However, the estimation of the cascaded channel depends on the RIS configuration, which implies that the mini-

mum required training periods equals the total number of configurations for each UE. Consequently, this estimation overhead becomes prohibitive as the numbers of UEs and RIS elements together with their configuration options increase [25]. Late interests in reducing the channel estimation overhead focus on efficient decompositions of the received signal [23] and on designing RIS configurations tailored for channel estimation [15]. In the vast majority of the CDS works, Time Duplex Division (TDD) is typically adopted and the CSI is assumed to be estimated in the uplink, and then, reused in the downlink. To this end, the coherence time is always considered to be long enough to cope with the channel training and uplink/downlink data transmission stages. Given the CSI availability, the BS computes the best pair of pre-coder/combiner as well as the set of RIS elements' configuration, which is communicated to the RIS via a side control link. This processing task is not straightforward due to the fact that a non-convex design optimization needs to be solved, increasing the operational complexity of the RIS-empowered communication system. When Orthogonal Frequency Division Multiplexing (OFDM) [26, 27] is taken into account, the complexity of the channel estimation and optimization scales with the number of subcarriers and UEs [22, 24, 16]. Several late studies have focused on accelerating this optimization using alternative methods at the expense of sacrificing the performance, such as suboptimal optimizations [1, 3, 28], or configuring sets of contiguous passive reflective elements with the same phase value to decrease the number of variables to be optimized [20, 21]. In addition, approaches based on RIS phase profile management are lately being investigated [29, 30, 31], which however still require certain estimations of channel parameters and sweeping over the available phase configurations.

Alternatively, random phase configurations at the RIS have been recently proposed [32, 33] in order to avoid the channel estimation of each passive element of the RIS and the complex optimization process. According to this scheme, the RIS elements are randomly configured at each symbol period, and hence, the multiple links produced provide a spatial diversity gain, and hence, the performance of the overall end-to-end link is improved. In previous work [32, 33], only theoretical bounds of the system in terms of outage probability and achievable rate were provided for the downlink case, assuming that any modulation and coding scheme can be applied. However, if CDS is chosen to be deployed, reference signals will be again needed to estimate the equivalent BS-UE channel and compute the pre-coder/combiner at the BS, similar to the case of massive MIMO.

The Non-CDS (NCDS) is an alternative demodulation scheme that does not require CSI, hence, it reduces the undesirable signaling overhead and increases the effective data rate of the communication system [34, 35, 36]. This scheme is realized with reduced complexity transmission and reception, which implies cheaper transceiver hardware devices and lower latency for processing. Recently, NCDS has been combined with massive Multiple-Input Multiple-Output (MIMO) systems [37, 38, 39, 40, 41, 42, 43], where it was shown to provide a significant performance gain compared to CDS for some 5G challenging scenarios, such as vehicular and low-latency communications. It was highlighted in [37, 38] that NCDS is more robust than CDS for low Signal-to-Noise Ratio (SNR) scenarios, where the latter scheme additionally suffers from noisy channel estimates. In [39, 40, 41, 42, 43], the use of differential Phase Shift Keying (PSK) [44] was proposed. Those works showcased that this modulation scheme is robust in very fast time-varying channels, because it only requires that the channel response is quasi-static over two contiguous symbols. Additionally, [40, 41, 42, 43] proved the superiority of NCDS over CDS in terms of throughput, due to the fact that reference signals designed for channel tracking can be fully avoided.

To the best of our knowledge, an RIS-empowered wireless communication scheme based on the combination of random phase rotations with NCDS have not been proposed yet. On the one hand, the exploitation of the spatial diversity offered by the random phase configurations circumvents the requirement for the estimation of large channel matrices involving the gains at the RIS elements as well as the complex RIS optimization process. On the other hand, the NCDS can fully avoid the estimation of the resulting channel between BS-UE, and hence, reduce the complexity produced by computing the precoder/combiner at the BS. Motivated by these facts, in this paper we propose the novel combination of the latter technologies targeting new broadband applications of 5G-Advanced and 6G systems, such as long-range communications (low SNR cases), vehicular communications (mobility scenarios), and low-latency communications. The main contributions of this paper are summarized as follows:

- We present a RIS-empowered Single-Input Multiple-Output (SIMO) OFDM system with random phase rotations at the RIS and differential PSK modulation. This combination requires neither channel estimation nor solving a non-convex optimization problem. Consequently, the channel training stage is no longer required and the side link to control the RIS is removed, since its passive elements are randomly configured. Hence, the proposed solution is not only able to improve the efficiency of the system by exploiting the spatial diversity produced by the RIS, but it is also capable of reducing the processing complexity, especially for broadband multi-carrier waveforms, hence, enabling the massive deployment of RISs.

- The Signal-to-Interference-plus-Noise Ratio (SINR), determining the useful signal over the self-interference and thermal noise terms, of the proposed RIS-empowered NCDS system is analytically characterized over both an Independent and Identically Distributed (IID) Rayleigh channel model and a realistic geometric wideband channel model

[45, 46, 47], including UE mobility, spatial correlations among closely located antenna elements and temporal correlations channel samples.

- Capitalizing on the approach of [43], we derive approximate analytical expressions for the Symbol Error Probability (SEP) of the proposed system, when operating under any of the two considered channel models.
- Our simulation results verify the accuracy of the presented analysis and highlight the superiority of the proposed NCDS system over a relevant CDS one. The inefficiency of the cascaded channel estimation for the CDS system is numerically assessed using the 5G numerology, which is an additional figure of merit to show its weakness as compared to the proposed NCDS approach. Interestingly, the performance of the proposed NCDS does not suffer from any performance penalization when low resolution quantization (even at 1 bit) is considered for the RIS phase configurations, unlike CDS.

The remainder of the paper is organized as follows. Section 2 introduces the system model and the two considered channel models. Section 3 details the implementation of the proposed differential PSK scheme and presents the analytical expressions for the SINR. Section 4 includes the approximate SEP analysis and Section 5 discusses the performance assessment results as compared to the CDS. Finally, Section 6 concludes the paper.

Notation: Matrices, vectors, and scalar quantities are denoted by boldface uppercase, boldface lowercase, and normal letters, respectively. $[\mathbf{A}]_{mn}$ denotes the element in the m-th row and n-th column of $\mathbf{A}$, $[\mathbf{A}]_{:,n}$ is $\mathbf{A}$'s n-th column, $\mathbf{v}_{\max}(\mathbf{A})$ is $\mathbf{A}$'s principal eigenvector, and $[\mathbf{a}]_n$ represents the n-th element of $\mathbf{a}$. $\mathrm{diag}(\mathbf{a})$ denotes a diagonal matrix whose diagonal elements are formed by $\mathbf{a}$'s elements. $\Re(\cdot)$ and $\Im(\cdot)$ represent the real and imaginary part of a complex number, respectively, and $\jmath$ is the imaginary unit, while $*$ denotes the convolution operation. $||\cdot||_F^2$ denotes the squared Frobenius norm. $|\cdot|$ is the absolute value. $\mathbb{E}\{\cdot\}$ represents the expected value of a random variable and $\mathcal{CN}(0,\sigma^2)$ represents the circularly-symmetric and zero-mean complex normal distribution with variance σ^2.

2. SYSTEM AND CHANNEL MODELS

This section describes the considered mobile communication link empowered by an RIS. In addition, the idealistic and realistic propagation channel models are detailed.

2.1 Considered mobile communication scenario

The considered mobile communication scenario comprises a BS, an RIS, and a single-antenna UE (see Fig. 1). The BS is equipped with a Uniform Rectangular Array

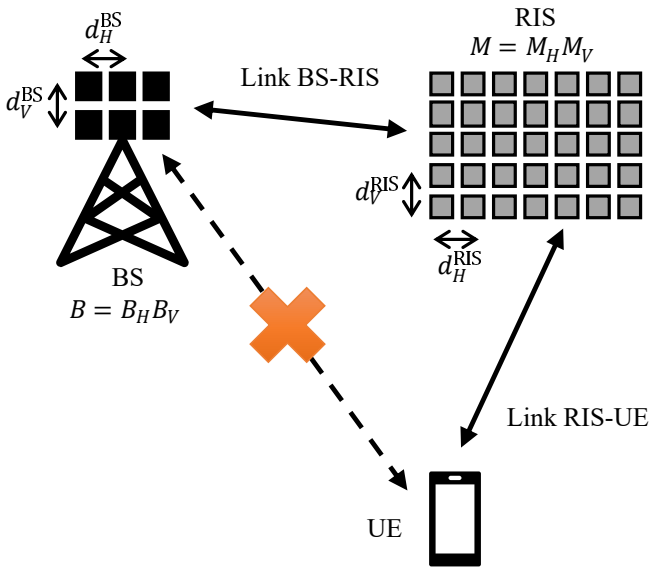

Fig. 1 – The RIS-empowered wireless communication link comprising a multi-antenna BS, a multi-element passive RIS, and a single-antenna mobile UE.

(URA) consisting of $B = B_H B_V$ antenna elements, where B_H and B_V denote the number of elements in the horizontal and vertical axes, respectively, and the distance between any two contiguous elements in their respective axes is given by d_H^{BS} and d_V^{BS}. Analogously to the BS, the RIS is built by $M = M_H M_V$ fully passive reflecting unit elements, whose respective distances between elements are given by d_H^{RIS} and d_V^{RIS}. The UE is constrained to have a single antenna element. Throughout the paper, different numbers B of antennas at the BS will be considered; a small value for B corresponds to a small and low-complexity BS, while a large B indicates that the BS is equipped with a massive MIMO array. On the other hand, the number M of passive elements at the RIS may be extremely large due its low fabrication and operational costs.

Regarding the signal propagation, it is assumed that a direct communication link between the BS and UE (BS-UE) is absent, due to the presence of blockages similar to [48, 49, 50]. Therefore, the communication between the BS and UE must be established through the RIS, via the BS-RIS and RIS-UE communication links. This work focuses on the uplink case, where the UE transmits both reference (if needed, e.g., in CDS) and data symbols to the BS through the RIS. It is understood that other UEs may be multiplexed in different orthogonal (time or frequency) resources; this extension is left for future work. It is assumed that, at each communication frame, the UE transmits a frame of N contiguous OFDM symbols of K subcarriers each. In order to avoid the Inter-Symbol and Inter-Carrier Interferences (ISI and ICI) due to the multipath, the length L_{CP} of the cyclic prefix must be long enough to absorb the effective multipath produced by the cascaded channel, namely the sum of the lengths of each of the channel responses of both BS-RIS and RIS-UE channels. The baseband representation of the received signal $\mathbf{y}_{k,n} \in \mathbb{C}^{B\times 1}$ at the BS in the k-th subcarrier, with

$1 \leq k \leq K$, and n-th OFDM symbol, with $1 \leq n \leq N$, is given by

$$\mathbf{y}_{k,n} = \mathbf{q}_{k,n} x_{k,n} + \mathbf{v}_{k,n}, \tag{1}$$

where $x_{k,n} \in \mathbb{C}$ denotes the symbol transmitted from the UE at the k-th subcarrier and n-th OFDM symbol, whose transmit power is $\mathbb{E}\left\{|x|^2\right\} = P_x$, $\mathbf{v}_{k,n} \in \mathbb{C}^{B\times 1}$ represents the Additive White Gaussian Noise (AWGN) vector which is distributed as $\left[\mathbf{v}_{k,n}\right]_b \sim \mathcal{CN}\left(0, \sigma_v^2\right)$, and $\mathbf{q}_{k,n} \in \mathbb{C}^{B\times 1}$ is the effective RIS-empowered cascaded channel frequency response, which can be decomposed for $1 \leq k \leq K$ and $1 \leq n \leq N$ as

$$\mathbf{q}_{k,n} \triangleq \mathbf{H}_{k,n} \boldsymbol{\Psi}_n \mathbf{g}_{k,n} = \sum_{m=1}^{M} \left[\boldsymbol{\psi}_n\right]_m \left[\mathbf{H}_{k,n}\right]_{:,m} \left[\mathbf{g}_{k,n}\right]_m, \tag{2}$$

where $\mathbf{H}_{k,n} \in \mathbb{C}^{B\times M}$ is the channel frequency response matrix between BS and RIS, $\mathbf{g}_{k,n} \in \mathbb{C}^{M\times 1}$ accounts for the channel frequency response vector between RIS and the single UE of interest, and $\boldsymbol{\Psi}_n \triangleq \text{diag}\left(\boldsymbol{\psi}_n\right) \in \mathbb{C}^{M\times M}$ is a diagonal matrix accounting for the effective phase configurations applied by the passive reflecting elements of the RIS at the n-th OFDM symbol, where $\boldsymbol{\psi}_n \in \mathbb{C}^M$ is defined as follows:

$$\boldsymbol{\psi}_n \triangleq \left[\exp\left(j\psi_{n,1}\right) \quad \cdots \quad \exp\left(j\psi_{n,M}\right)\right], \tag{3}$$

with $\psi_{n,m}$ for $1 \leq m \leq M$ representing the phase shift of the m-th passive element of the RIS panel.

2.2 Independent and Identically Distributed (IID) channel model

As a benchmark, we consider the case where the elements of the channel frequency response for both links (BS-RIS and RIS-UE) are IID. This channel model will be used for the purpose of upper-bounding the performance of the proposed NCDS, and comparing it with a more realistic geometric wideband channel model. In this case, the propagation channels (BS-RIS and RIS-UE) at the k-th subcarrier and n-th OFDM symbol are modeled as

$$\mathbf{H}_{k,n} \triangleq \sqrt{L_\alpha}\mathbf{A}_{k,n}, \quad \left[\mathbf{A}_{k,n}\right]_{bm} \sim \mathcal{CN}\left(0, \sigma_\alpha^2\right), \tag{4}$$

$$\mathbf{g}_{k,n} \triangleq \sqrt{L_\beta}\mathbf{b}_{k,n}, \quad \left[\mathbf{b}_{k,n}\right]_m \sim \mathcal{CN}\left(0, \sigma_\beta^2\right), \tag{5}$$

$$1 \leq b \leq B, \quad 1 \leq m \leq M,$$

where L_α and L_β denote the large-scale gains of the BS-RIS and RIS-UE links, respectively, and $\mathbf{A}_{k,n} \in \mathbb{C}^{B\times M}$ and $\mathbf{b}_{k,n} \in \mathbb{C}^{M\times 1}$ model the small-scale fading for their respective channels, according to a Rayleigh distribution. Hence, the average gain of each link is $\sigma_h^2 = L_\alpha \sigma_\alpha^2$ and $\sigma_g^2 = L_\beta \sigma_\beta^2$, respectively.

Moreover, it is assumed that the channel between the BS and RIS remains quasi-static, while the channel between the RIS and UE may suffer from time variability. The temporal correlation is characterized by the Jake's model [**rappa**], and can be expressed as follows:

$$\mathbb{E}\left\{\left(\left[\mathbf{g}_{k,n}\right]_m\right)^* \left[\mathbf{g}_{k,n'}\right]_m\right\} = \left|J_0\left(2\pi f_d \frac{\Delta n}{\Delta f}\left(1 + \frac{L_{CP}}{K}\right)\right)\right|, \tag{6}$$

$$\Delta n = n' - n, \quad 1 \leq k \leq K, \quad 1 \leq n \leq N, \quad 1 \leq m \leq M,$$

where $J_0(\cdot)$ denotes the zero-th order Bessel function of the first kind [51], and f_d and Δf represent the Doppler frequency shift experienced by the signal transmitted from the UE and the distance between two contiguous subcarriers, respectively, both measured in Hz.

2.3 Geometric wideband channel model

For a more realistic performance evaluation, the two links (BS-RIS and RIS-UE) are characterized with a geometric wideband model [45, 46, 47], made up of the superposition of several separate clusters, where each of them has a different value of delay and gain. Moreover, each cluster is comprised of a certain number of rays with different angles of arrival and departure. The delays and geometrical positions of each cluster/ray are typically characterized by the Delay Spread and Angular Spread (DS and AS), respectively. Each propagation model has its own definition for the value of these parameters, the number of clusters/rays and how the delays and rays are distributed for a given propagation environment. Then, given the information of these clusters/rays, the array steering vectors of both transmitter and receiver are included to model the spatial correlation due to the array responses. Therefore, note that this channel model is able to account for the spatial correlation considering both the given antenna array response of the BS and RIS, as well as the geometrical positions of all clusters/rays.

In order to provide a realistic evaluation of the system, the propagation channel model recommended for 5G [7] is chosen, where it is assumed that all clusters have the same number of rays and all the rays of a particular cluster have the same delay and gain. The power-delay profile follows an exponential distribution whose standard deviation is the DS; the azimuth angles of arrival/departure are modeled by a wrapped Gaussian distribution which is characterized by the Azimuth angular Spread of Arrival and Azimuth angular Spread of Departure (ASA and ASD); and the zenith angles of arrival/departure are modeled by a Laplacian distribution, also characterized by the Zenith angular Spread of Arrival and Zenith angular Spread Departure (ZSA and ZSD).

The channel response between the BS and RIS at the k-th subcarrier and n-th OFDM symbol can be described as

$$\mathbf{H}_{k,n} \triangleq \sqrt{L_\alpha} \sum_{c=1}^{C_\alpha} \sum_{r=1}^{R_\alpha} \alpha_n^{cr} \mathbf{a}_{\text{BS}}\left(\phi_n^{cr}, \theta_n^{cr}\right) \mathbf{a}_{\text{RIS}}^H\left(\bar{\varphi}_n^{cr}, \bar{\vartheta}_n^{cr}\right) \times$$
$$\times \exp\left(-j\frac{2\pi}{K}\left(k-1\right)\tau_{\alpha_n}^{\,c}\right), \quad \alpha_n^{cr} \sim \mathcal{CN}\left(0, \frac{\sigma_{\alpha,c}^2}{R_\alpha}\right), \tag{7}$$

where C_α is the number of clusters, R_α represents the number of rays for each cluster, ${\tau_\alpha}_n^c$ accounts for the delay of the c-th cluster measured in samples, α_n^{cr} is the channel coefficient for the c-th cluster and r-th ray, $\sigma_{\alpha,c}^2$ is the average gain of the c-th cluster, and $\mathbf{a}_{\text{BS}}\left(\phi_n^{cr}, \theta_n^{cr}\right)$ accounts for the array steering vector at the BS, and its arguments are the azimuth and elevation angles of arrival, respectively, for the c-th cluster and r-th ray. The steering vector for the BS is given by

$$\begin{aligned}&\left[\mathbf{a}_{BS}\left(\phi,\theta\right)\right]_{B_H(b_V-1)+b_H} = \\ &\exp\left(\jmath\frac{2\pi}{\lambda}(b_H-1)d_H^{\text{BS}}\sin\left(\theta\right)\cos\left(\phi\right)\right)\times \\ &\exp\left(\jmath\frac{2\pi}{\lambda}(b_V-1)d_V^{\text{BS}}\sin\left(\theta\right)\sin\left(\phi\right)\right), \\ &1\le b_H\le B_H,\quad 1\le b_V\le B_V,\end{aligned} \tag{8}$$

where λ is the wavelength. Similar to the BS, $\mathbf{a}_{\text{RIS}}\left(\bar{\varphi}_n^{cr}, \bar{\vartheta}_n^{cr}\right)$ denotes the steering vector for the RIS, and its arguments are the azimuth and elevation angles of departure, respectively, for the c-th cluster and r-th ray. The expression for the steering vector is the same as described in (*(8)*), replacing respectively the set (B_H, B_V, d_H^{BS}, d_V^{BS}) by the set (M_H, M_V, d_H^{RIS}, d_V^{RIS}).
The channel response between the RIS and UE at the k-th subcarrier and n-th OFDM symbol is given by

$$\begin{aligned}&\mathbf{g}_{k,n} \triangleq \sqrt{L_\beta}\sum_{c=1}^{C_\beta}\sum_{r=1}^{R_\beta}\beta_n^{cr}\mathbf{a}_{\text{RIS}}\left(\varphi_n^{cr},\vartheta_n^{cr}\right)\times \\ &\times\exp\left(-j\frac{2\pi}{K}\left(k-1\right){\tau_\beta}_n^c\right),\quad \beta_n^{cr}\sim\mathcal{CN}\left(0,\frac{\sigma_{\beta,c}^2}{R_\beta}\right),\end{aligned} \tag{9}$$

where C_β is the number of clusters, R_β represents the number of rays for each cluster, ${\tau_\beta}_n^c$ accounts for the delay of the c-th cluster measured in samples, α_n^{cr} is the channel coefficient for the c-th cluster and r-th ray, $\sigma_{\beta,c}^2$ is the average gain of the c-th cluster, $\mathbf{a}_{\text{RIS}}\left(\varphi_n^{cr}, \vartheta_n^{cr}\right)$ accounts for the array steering vector at the RIS, and its arguments are the azimuth and elevation angles of arrival, respectively, for the c-th cluster and r-th ray. Hence, similar to the IID channel model, the average gain of each link can be defined as

$$\sigma_h^2 = L_\alpha\sum_{c=1}^{C_\alpha}\sigma_{\alpha,c}^2,\quad \sigma_g^2 = L_\beta\sum_{c=1}^{C_\beta}\sigma_{\beta,c}^2. \tag{10}$$

Similar to the IID channel model case, the link between RIS and the UE of interest may suffer from a Doppler shift due to the mobility also charaterized by (*(6)*), while the link between BS and RIS is assumed to be quasi-static.

3. PROPOSED RIS-EMPOWERED SYSTEM BASED ON NCDS WITH DIFFERENTIAL MODULATION

Different work in the literature has proposed the classical CDS to exploit the RIS-empowered communication link. However, as we mentioned, it requires long channel training and very complex optimization processes, while the former is aiming to obtain the CSI for each passive element of the RIS per UE, and the latter is in charge of getting the best phase configuration at the RIS and the precoder/combiner at the BS. In order avoid these inefficiencies, this work proposes to replace the classical CDS by an NCDS based on differential modulation, and it also makes use of random phase rotations at the RIS in order to exploit the spatial diversity [52]. This approach does not require training-based channel estimation in order to perform the demodulation and decision, as shown in [39, 40, 41, 42, 43]. Besides, the complex optimization processes are also skipped since the RIS are randomly configured [52].

3.1 Differential encoding and decoding

At the UE, the data symbols are differentially encoded in the time domain before their transmission as:

$$x_{k,n} = \begin{cases} s_{k,n}, & n=1 \\ x_{k,n-1}s_{k,n}, & 2\le n\le N\end{cases},\quad 1\le k\le K. \tag{11}$$

where $s_{k,n}$ denotes the complex symbol to be transmitted at the k-th subcarrier and n-th OFDM symbol, that belongs to a PSK constellation and its power is normalized (i.e., $\left|s_{k,n}\right|^2 = 1$). Note that the differential modulation only requires a single reference symbol $s_{k,1}$ at the beginning of the burst in order to allow the differential demodulation, which represents a negligible overhead. The differential modulation can be also implemented in the frequency domain with the same performance [40]. Before data transmission, the power of differential symbols x_k^n is scaled according to P_x.
Given (*(1)*), the BS performs the differential decoding as

$$z_{k,n} = \frac{1}{MB}\left(\mathbf{y}_{n-1}^k\right)^H\mathbf{y}_{k,n} = \frac{1}{MB}\sum_{i=1}^{4}I_i, \tag{12}$$

$$2\le n\le N,\quad 1\le k\le K,$$

$$I_1 = \left(\mathbf{q}_{n-1}^k\right)^H\mathbf{q}_{k,n}s_{k,n},\quad I_2 = \left(\mathbf{q}_{n-1}^k x_{n-1}^k\right)^H\mathbf{v}_{k,n}, \tag{13}$$

$$I_3 = \left(\mathbf{v}_{n-1}^k\right)^H\mathbf{q}_{k,n}x_{k,n},\quad I_4 = \left(\mathbf{v}_{n-1}^k\right)^H\mathbf{v}_{k,n}, \tag{14}$$

where I_1 includes the useful symbol $s_{k,n}$ to be decided, however, it is polluted by the effective RIS-empowered cascaded channel. In addition, I_2 and I_3 represent the cross-interference terms produced by the noise and the received differential symbol in two time instants, while I_4 is exclusively produced by the product of the noise in two instants. The symbol decision is performed over the variable $z_{k,n}$ in *(12)*. Note that the proposed NCDS does not require obtaining the CSI, and hence, the undesirable cascaded channel sounding task can be avoided. To this end, in this paper, we consider any random configuration $\mathbf{\Psi}_n$ such that $\psi_{n,m}\sim\mathcal{U}\left[0,2\pi\right]$ for the RIS passive elements, avoiding the overhead to solve any complex optimization problem and then feed back the optimized parameters to

the RIS, as in the baseline CDS case. Note that $\mathbf{\Psi_n}$ can be randomly set for each OFDM symbol without any restriction (unlike in CDS), however, the continuous configuration of the RIS may unnecessarily increase the energy and/or resource consumption. Hence, it is recommended to update these phase configurations at each data frame (e.g. every N OFDM symbols). It will be shown in the performance evaluation results that the proposed NCDS-based approach provides substantial gains over the baseline CDS, both in terms of computational complexity and achievable performance.

3.2 Analysis of the SINR for the IID channel model

According to *(12)-(14)*, there are interference and noise terms produced by the differential decoding. The received symbol $z_{k,n}$ should be compared to the transmitted symbol $s_{k,n}$ in order to characterize these undesirable effects, which can be expressed as

$$\mathbb{E}\left\{\left|\sigma_h^2\sigma_g^2 s_{k,n}-z_{k,n}\right|^2\right\}=\sigma_h^4\sigma_g^4P_x^2+\mathbb{E}\left\{\left|z_{k,n}\right|^2\right\}- \\ -2\sigma_h^2\sigma_g^2\Re\left\{\mathbb{E}\left\{\left(s_{k,n}\right)^H z_{k,n}\right\}\right\}, \tag{15}$$

where the expectation is performed over the subcarriers and OFDM symbols. According to [42], the four terms given in *(13)* and *(14)* are statistically independent due to the fact that the channel frequency response, noise, and symbols are independent random variables, and the noise samples between two time instants are also independent. Hence, the two terms in (*(15)*) can be simplified as

$$\mathbb{E}\left\{\left|z_{k,n}\right|^2\right\}=\frac{1}{M^2B^2}\sum_{i=1}^{4}\mathbb{E}\left\{\left|I_i\right|^2\right\}, \tag{16}$$

$$\mathbb{E}\left\{\left(s_{k,n}\right)^H z_{k,n}\right\}=\frac{1}{MB}\mathbb{E}\left\{\left(s_{k,n}\right)^H I_1\right\}, \tag{17}$$

and the SINR of the proposed NCDS approach, which is denoted by ρ_{iid}, can be defined as

$$\frac{1}{\rho_{\text{iid}}}=1+\frac{1}{M^2B^2\sigma_h^4\sigma_g^4P_x^2}\sum_{i=1}^{4}\mathbb{E}\left\{\left|I_i\right|^2\right\}- \\ -\frac{2}{MB\sigma_h^2\sigma_g^2P_x^2}\Re\left\{\mathbb{E}\left\{\left(s_{k,n}\right)^H I_1\right\}\right\}. \tag{18}$$

Assuming the IID Rayleigh channel model, each of the expected values in *(18)* can be expressed as:

$$\mathbb{E}\left\{\left(s_{k,n}\right)^H I_1\right\}=P_x^2B\sigma_h^2M\sigma_g^2,\quad \mathbb{E}\left\{\left|I_4\right|^2\right\}=B\sigma_v^4, \tag{19}$$

$$\mathbb{E}\left\{\left|I_1\right|^2\right\}=P_x^2(1+B)B\sigma_h^4(1+M)M\sigma_g^4, \tag{20}$$

$$\mathbb{E}\left\{\left|I_2\right|^2\right\}=\mathbb{E}\left\{\left|I_3\right|^2\right\}=\sigma_v^2P_xB\sigma_h^2M\sigma_g^2. \tag{21}$$

Substituting *(19)-(21)* into *(18)*, yields the following expression for the SINR of the proposed NCDS approach:

$$\rho_{\text{iid}}=\frac{MB}{B+M+1+\frac{2\sigma_v^2}{\sigma_h^2\sigma_g^2P_x}+\frac{\sigma_v^4}{\sigma_h^4\sigma_g^4P_x^2M}}, \tag{22}$$

which indicates that not only the number B of the BS antennas improves the system performance, but also the number M of the RIS passive elements helps to reduce the interference and noise terms, by providing an additional spatial diversity gain. Consequently, the RIS is able to improve the overall performance of the system. Furthermore, as clearly indicated from the numerator of *(22)*, the performance of the system will be high, even though the number of antennas (B) and/or the number of passive elements of the RIS (M) are not very large, since these values are multiplied.

3.3 Analysis of the SINR for the geometric wideband channel model

Similar to the previous subsection, each of the expected values in *(18)* for the geometric wideband channel model are as follows:

$$\mathbb{E}\left\{\left|I_1\right|^2\right\}=P_x^2Q_4,\quad \mathbb{E}\left\{\left(s_{k,n}\right)^H I_1\right\}=P_x^2Q_2, \tag{23}$$

$$\mathbb{E}\left\{\left|I_2\right|^2\right\}=\mathbb{E}\left\{\left|I_3\right|^2\right\}=P_x\sigma_v^2Q_2 \tag{24}$$

where the terms Q_4 and Q_2 are defined as

$$Q_4\triangleq 4L_\alpha^2L_\beta^2 \\ \times\sum_{c_\alpha=1}^{C_\alpha}\frac{\sigma_{\alpha_c}^4}{R_\alpha^2}\sum_{r_\alpha=1}^{R_\alpha}\sum_{c_\beta=1}^{C_\beta}\frac{\sigma_{\beta_c}^4}{R_\beta^2}\sum_{r_\beta=1}^{R_\beta}\mathbb{E}\left\{\left|\tilde{\mathbf{a}}_n\left(c_\beta,r_\beta,c_\alpha r_\alpha\right)\right|^4\right\}, \tag{25}$$

$$Q_2\triangleq L_\alpha L_\beta \\ \times\sum_{c_\alpha=1}^{C_\alpha}\frac{\sigma_{\alpha_c}^2}{R_\alpha}\sum_{r_\alpha=1}^{R_\alpha}\sum_{c_\beta=1}^{C_\beta}\frac{\sigma_{\beta_c}^2}{R_\beta}\sum_{r_\beta=1}^{R_\beta}\mathbb{E}\left\{\left|\tilde{\mathbf{a}}_n\left(c_\beta,r_\beta,c_\alpha r_\alpha\right)\right|^2\right\}, \tag{26}$$

and $\tilde{\mathbf{a}}_n\left(c_\beta,r_\beta,c_\alpha r_\alpha\right)$ denotes the joint spatial correlation of the BS and RIS.

When comparing *(23)-(26)* with *(19)-(21)* it turns out that the spatial correlation is upper bounded by the IID case as:

$$\frac{\mathbb{E}\left\{\left|\tilde{\mathbf{a}}_n\left(c_\beta,r_\beta,c_\alpha r_\alpha\right)\right|^2\right\}}{MB}\le 1, \tag{27}$$

$$\frac{4\mathbb{E}\left\{\left|\tilde{\mathbf{a}}_n\left(c_\beta,r_\beta,c_\alpha r_\alpha\right)\right|^4\right\}}{M^2B^2}\le 1+\frac{B+M+1}{MB}. \tag{28}$$

Substituting *(23)-(26)* in *(18)*, the SINR is obtained as

$$\frac{1}{\rho_{\text{geo}}}=1+\frac{Q_4}{M^2B^2\sigma_h^4\sigma_g^4}-\frac{2Q_2}{MB\sigma_h^2\sigma_g^2}+ \\ +\frac{1}{M^2B^2\sigma_h^4\sigma_g^4}\left(\frac{2Q_2\sigma_v^2}{P_x}+B\sigma_v^4\right)\ge\frac{1}{\rho_{\text{iid}}}. \tag{29}$$

Obviously, the spatial correlation of the antennas at the BS and the RIS passive elements is limiting the performance of the system for this geometric wideband channel model as compared to the IID case. Again, similar to *(22)*, both the number of antennas at the BS (B) and the number of passive elements (M) are contributing to enhance the SINR in *(29)*.

4. ERROR PROBABILITY AND COMPLEXITY ANALYSES

In this section, we first present analytical expressions for the SEP performance of the proposed RIS-empowered communication system that is based on NCDS. Then, the complexities of the proposed NCDS system and the baseline CDS, as detailed in Section 3, are discussed.

4.1 Symbol Error Probability (SEP) analysis

The analysis of an approximated SEP is given in this section to characterize the performance of the proposed NCDS. Reference [43] has provided an asymptotic analysis for this purpose assuming that the number of the antennas at the BS is very large and assuming only an IID channel model. Therein, the Probability Density Function (PDF) of the decision variable $z_{k,n}$ is approximated as a complex normal distribution. However, this approximation is not very realistic when the number of BS antennas is not large.

Taking into account the analytical expressions for I_1, I_2, I_3, and I_4 given in *(13)* and *(14)*, it holds that the first term depends only on the channel and it is a real random variable, while the rest of the terms depend on the noise and they are complex random variables. Hence, the PDF of $z_{k,n}$ can be approximated as

$$f_{z_{k,n}}(u,v) \approx f_{I_1}(u) * f_{I_2,I_3,I_4}(u,v), \qquad (30)$$

where $f_{I_1}(u)$ is the PDF of I_1, $f_{I_2,I_3,I_4}(u,v)$ is the joint PDF of I_2, I_3 and I_4, and the variables u and v correspond to the real and imaginary parts of $z_{k,n}$, respectively. As shown in [43], the latter joint PDF can be accurately approximated by a zero-mean complex normal distribution with variance

$$\sigma_s^2 = \sum_{i=2}^{4} \mathbb{E}\left\{|I_i|^2\right\} = B\sigma_v^2\left(\sigma_v^2 + 2P_x\sigma_h^2 M\sigma_g^2\right), \qquad (31)$$

while the PDF expression $f_{I_1}(u)$ depends on the chosen propagation channel model.

For the IID channel model, the scalar product $\left(\mathbf{q}_{n-1}^k\right)^H \mathbf{q}_{k,n}$ is a sum of B statistically independent terms (due to the lack of spatial correlation), where each term's distribution can be accurately approximated by $\mathcal{N}\left(0, \mathbb{E}\left\{|I_1|^2\right\}\right)$ when M is large enough; this holds from the Central Limit Theorem (CLT) [**clt**]. Hence, the PDF of the term I_1 can be approximated by

$$\begin{aligned} f_{I_1}(u) &\approx \Gamma\left(B, \mathbb{E}\left\{|I_1|^2\right\}\right) \\ &= \Gamma\left(B, P_x^2(1+B)B\sigma_h^4(1+M)M\sigma_g^4\right). \end{aligned} \qquad (32)$$

Table 1 – Complexity comparison between the proposed NCDS and the considered baseline CDS

	System Opt. Complexity	**Total Num. of Complex Products**
CDS [53]	$\mathcal{O}\left(R_t(B^3+M)K\right)$	BK
NCDS	–	$(B+1)(K-1)$

On the other hand, for the case of the geometric wideband channel model, there exists spatial correlation among the BS antenna elements and the RIS passive elements. By assuming that the number of clusters/rays is large enough, thus the CLT holds, $f_{I_1}(u)$ can be approximated by a zero-mean normal distribution with variance $\mathbb{E}\left\{|I_1|^2\right\}$. Therefore, *(30)* can be approximated by a zero-mean normal distribution with variance σ_z^2, which can be derived as

$$\begin{aligned} \sigma_z^2 =& P_x^2(1+B)B\sigma_h^4(1+M)M\sigma_g^4 \\ &+ B\sigma_v^2\left(\sigma_v^2 + 2P_x\sigma_h^2 M\sigma_g^2\right). \end{aligned} \qquad (33)$$

The SEP of the decision variable $z_{k,n}$ for the k-th subcarrier of each n-th OFDM symbol, assuming without loss of generality that the transmitted symbol is $s_{k,n} = 1$, can be computed from the following double-integral

$$\begin{aligned} P_e &= 1 - \int_0^{\infty} \int_{\mathcal{D}_u} f_{z_{k,n}}(u,v)\mathrm{d}v\mathrm{d}u, \\ \mathcal{D}_u &\in u\tan\left(\frac{\pi}{M_q}\right)[-1,1], \end{aligned} \qquad (34)$$

where $\mathcal{D}_u$ denotes the decision region for the particular symbol of interest and M_q is the number of the symbols in the PSK constellation. Since *(34)* is hard, if not impossible, to be expressed in a closed form, it will be evaluated numerically in the next performance assessment section.

4.2 Complexity analysis

The complexity evaluation for both CDS and NCDS before detection are summarized in Table 1. The proposed NCDS does not require solving any complex optimization problem, since we consider a random phase configuration for the RIS. For the differential encoding, the transmitter (i.e., the UE) requires $K-1$ complex products at each OFDM symbol, where the receiver (i.e., BS) needs the same number of complex products for the differential decoding at each RF chain before the symbol decision [41], resulting in the total of $B(K-1)$ products.

On the contrary, the CDS not only requires complex products for performing the post-coding, but it also requires solving the optimization problem for the BS combining vector and the RIS phase configuration. Different suboptimal methods can be proposed to avoid the complexity issue, at the expense of decreasing the overall performance. In order to constrain the complexity, the considered baseline CDS implements the iterative method of [53], whose complexity linearly scales with the number of algorithmic iterations required iterations, R_t, the number M of RIS

Table 2 – Simulation parameters

BS loc.	(0,0,3)	$\mathbf{f_c}$	3.5 GHz	**ASD**	7º, 30º
RIS loc.	(3,0,3)	$\mathbf{\Delta f}$	30 KHz	**ASA**	12º, 50º
UE loc.	(6,1,1)	$\mathbf{K}$	1024	**ZSD**	25º, 130º
$\mathbf{L_\alpha}$	-48 dB	$\boldsymbol{\sigma_v^2}$	-116 dBW	**ZSA**	30º, 150º
$\mathbf{L_\beta}$	-59 dB	$\mathbf{N}$	140 symb.	**DS**	0.15 ms

passive elements, and the number K of OFDM subcarriers. It is noted that the CDS complexity increases severely with the number of BS antennas (it depends on B^3), which indicates that a massive MIMO BS is not recommended in RIS-empowered systems based on CDS.

5. PERFORMANCE EVALUATION RESULTS

In this section, several numerical results are provided in order to show the performance of the proposed NCDS, as compared to the considered baseline CDS, and the accuracy of the analytical results. A summary of the simulation parameters is provided in Table 2, the location of each network node is given by the Cartesian coordinates (x, y, z) measured in meters, and f_c denotes the carrier frequency. The channel propagation model adopted for the simulation results corresponds to the 3GPP factory scenario of size (60m,120m,3m), with the goal to evaluate the 5G performance [7]. The DS and AS were set the same values for both BS-RIS and RIS-UE channel links. Moreover, we have considered two values for each AS, where the lower values are denoted as the low AS scenario, while the higher values refer to the high AS scenario. Regarding the phase configurations for NCDS, these values are randomly chosen and set to the RIS for each frame (N contiguous OFDM symbols), regardless of the coherence time.

5.1 Baseline RIS-empowered system based on CDS

We detail the considered baseline RIS-empowered system that is based on conventional CDS. The performance of this reference system will be compared with that based on the proposed NCDS, which will be presented in the following section. According to [20, 21, 18, 22], in order to be able to fully exploit the benefits of the RIS, the system requires performing a channel training stage before the data transmission stage. This channel training stage mainly consists of three tasks: cascaded channel sounding, optimization for the desired RIS configuration, and parameter feedback. Moreover, in most of the previous works [1, 4, 3, 25, 54, 53], it has been assumed for the purpose of CDS for the RIS-empowered link that the coherence time (T_c), is always long enough so that the duration of channel training does not penalize the duration of the data transmission stage. However, even with low mobility, the cascaded channel will suffer from a certain time variability and its estimation must be periodically updated. Consequently, the pre-coder/combiner and RIS phase configuration need to be updated accordingly.

In order to take into account the inefficiency produced by the channel training stage, it is assumed that the data rate penalty due to channel sounding is lower-bounded by taking only into account the channel sounding time, since the feedback time is typically assumed to be negligible, and the optimization time is difficult to quantify due to the fact that the time required for solving the design optimization problem depends on the chosen numerical method and the amount of resources assigned for this task. Following [**rappa**], the coherence time measured in seconds is given by $T_c = 0.423/f_d$ and the coherence time measured in the number of OFDM symbols, N_c, can be computed as

$$N_c = \frac{\Delta f}{f_d}\frac{0.423K}{K + L_{CP}}. \tag{35}$$

The effective transmitted power at the UE can be defined as $P_x^{\text{eff}} \triangleq \frac{P_x}{\eta_c}$, where η_c represents the efficiency factor that takes into account the coherence time and the number of RIS passive elements to be sounded. This efficiency factor is given by

$$\eta_c \triangleq 1 - \frac{T_r}{T_c} \leq 1 - \frac{M}{N_c}, \tag{36}$$

where T_r is the period of time devoted for channel estimation. According to [25], the time and/or power resources devoted for performing the cascaded channel sounding are penalizing the overall performance of the system.

5.2 Verification of the analysis for the proposed NCDS

Fig. 2 illustrates the SINR performance as a function of the UE transmit power P_x in dBW of the proposed NCDS with 8-DPSK for both the IID Rayleigh and the geometric wideband channel models, considering $B = 2 \times 2$ antennas at the BS and different values M for the number of RIS passive elements. As clearly shown, the performance for the IID channel model corresponds to the best case for all simulated M values. On the other hand, for the particular case of a geometric wideband channel, the performance depends on the spatial correlation. When the angular positions of the clusters/rays are separated (i.e., high AS), the performance is better compared to the low AS case. Evidently, the improvement becomes even better for high numbers of M. It is also shown in this figure that the SINR analysis given in *(22)* and *(29)*, shown with black solid lines, accurately characterizes the RIS-empowered system performance.

The SEP of 4-DPSK modulation for the proposed NCDS is demonstrated in Fig. 3 for both considered channel models with $B = 4 \times 4$, high AS, and different values for M. Note that a symbol-by-symbol detection is performed after the differential decoder. The conclusions regarding this performance follow the trends of Fig. 2. A larger value for M (i.e., an RIS with more passive elements) results in improved performance and the IID channel yields better performance than the geometric one. The approximated

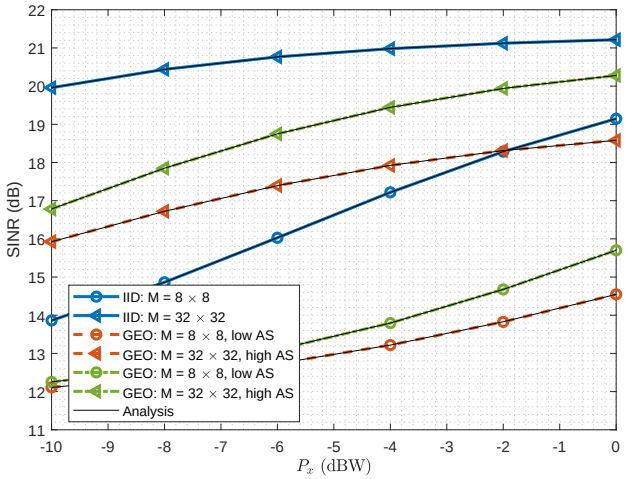

Fig. 2 – SINR performance in dB of the proposed NCDS for the IID Rayleigh and the geometric wideband channel models for various values M of the RIS passive elements, AS, and for $B = 2 \times 2$ BS antenna elements.

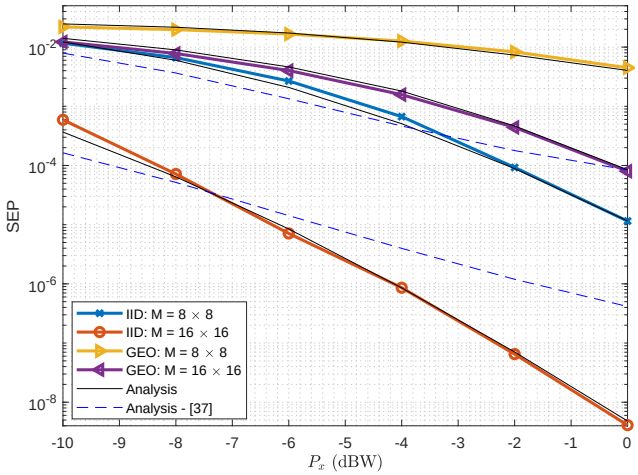

Fig. 3 – SEP performance of the proposed NCDS with 4-DPSK for the IID Rayleigh and the geometric wideband channel models. Various values M for the RIS passive elements, $B = 4 \times 4$ BS antennas, as well as high AS (ASD=30°, ASA=50°, ZSD=130°, and ZSA=150°) have been considered.

SEP provided by Section 4.1 is also plotted in the figure, showcasing that the analysis is accurate enough. Furthermore, for the particular case of the IID channel model, the proposed approximation is better than the one given in [43].

5.3 Evaluation of the efficiency factor for the baseline CDS

The efficiency factor for the considered baseline CDS, as defined in (*(36)*), is evaluated considering the parameters given in Table 2, which are taken from the 5G numerology [7]. The CSI of the cascaded channel is obtained hypothetically assuming that the first M OFDM symbols out of N_c (coherence time) are exclusively devoted for reference signal transmission. This is a larger overhead than supported in the 5G standard, but, as explained in Section 5.1, it is the minimum that allows a CDS-based RIS. In Table 3, the efficiency factor is numerically evaluated for various values M of the number of the RIS passive elements and UE speeds according to *(36)*. As indicated, an RIS equipped with large numbers of elements can be only applied in scenarios without or with very low mobility, while an RIS with small numbers of elements can be exploited in scenarios with some mobility. It is noted that the exploitation of an RIS with large M values using CDS will also have a negative impact on the system complexity.

5.4 Performance comparisons between NCDS and CDS

The SEP performance comparison between the proposed NCDS and the considered baseline CDS for 4-DPSK and QPSK modulations, respectively, and using a geometric wideband channel with low AS is illustrated in Fig. 4. To perform a fair comparison between the two schemes, we have defined the efficiency factor as follows

$$\eta = \begin{cases} 1, & \text{NCDS} \\ \eta_c, & \text{CDS} \end{cases} . \qquad (37)$$

This highlights that the proposed NCDS does not suffer any penalization (unlike CDS). Also, it can be deployed at any mobility scenario, exploiting the fact that the differential modulation can be implemented in the frequency dimension, as shown in [40, 41, 43]. As also concluded from Table 3, the proposed NCDS significantly outperforms CDS for large M values for the number of RIS passive elements. Moreover, even for the small M values, the NCDS outperforms CDS, due to the fact that the latter is not able to obtain accurate channel estimates due to the presence of noise (MSE=σ_v^2). This happens because the UE's transmit power is in general limited, as also are the amount of resources that can be devoted for CSI estimation while maintaining a reasonable efficiency.

5.5 Enabling practical large RIS with NCDS

The SEP of the proposed NCDS with 2-DPSK signaling is depicted in Fig. 5 for different values M for the number of RIS elements and B for the the BS antennas, and using a geometric wideband channel model with high AS. It is shown that if any of B and M increases, the NCDS performance improves. It is also evident from the two sets of results with the same MB product each that, it is preferable to have a larger M value rather than increasing B. Recall that in the proposed NDCS, the RIS phase configurations are randomly chosen, and a higher number M of RIS elements will increase the probability to adequately reflect the signal from the UE to BS.

In practical RIS implementations [4, 28], the phase configurations are constrained to finite sets, since the phase resolution of each RIS element is of the order of a few bits. In Fig. 5, we also consider one-bit quantization of the random phase configuration per data frame, i.e., the

Table 3 – Efficiency factor for the baseline CDS

	3 km/h	10 km/h	20 km/h	30 km/h	40 km/h
$\mathbf{M = 16}$	0.9738	0.9126	0.8242	0.7377	0.6522
$\mathbf{M = 32}$	0.9475	0.8251	0.6484	0.4754	0.3043
$\mathbf{M = 64}$	0.8951	0.6503	0.2967	0	0
$\mathbf{M = 128}$	0.7902	0.3005	0	0	0
$\mathbf{M = 256}$	0.5803	0	0	0	0
$\mathbf{M = 512}$	0.1607	0	0	0	0
$\mathbf{M = 1024}$	0	0	0	0	0

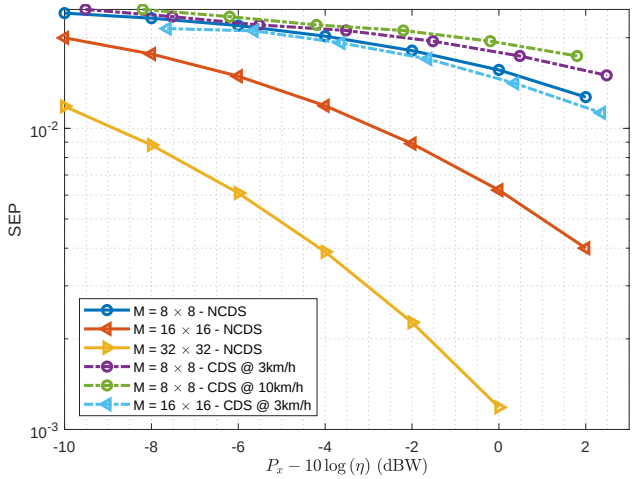

Fig. 4 – SEP performance comparison between the proposed NCDS and the baseline CDS for 4-DPSK and QPSK, respectively, various numbers M for the RIS elements, $B = 2 \times 2$ BS antennas, and using a geometric wideband channel model with low AS (ASD=7°, ASA=12°, ZSD=25°, and ZSA=30°).

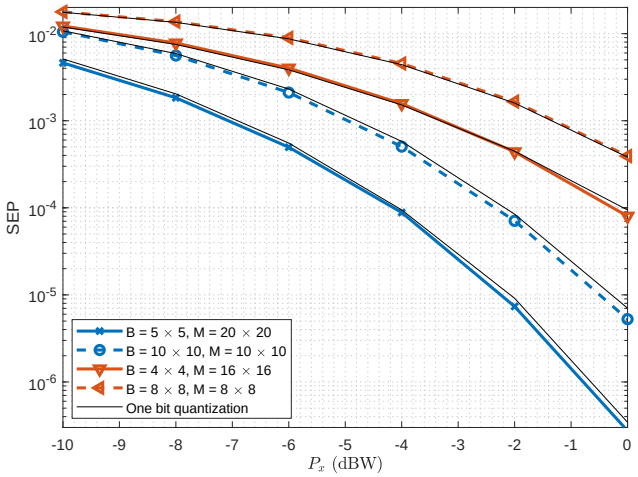

Fig. 5 – SEP performance of the proposed NCDS with 4-DPSK for different values M for the RIS elements and B for the the BS antennas, using a geometric wideband channel model with high AS (ASD=30°, ASA=50°, ZSD=130°, and ZSA=150°). Both random RIS phase configurations and their one-bit quantizations have been simulated.

phase configurations are randomly obtained from the set of predefined phases ($\psi_{n_1,m} = \psi_{n_2,m} \in \mathcal{A} = \{0, \pi\}$, $1 \leq n_1, n_2 \leq N$). It can be seen, that this quantization does not affect the NCDS performance, due to the fact that the proposed scheme combines non-coherently all received signals from the RIS, and neither channel estimation nor phase configuration optimization are required.

6. CONCLUSIONS

This paper presented an NCDS based on differential decoding combined with random RIS phase configurations, as an appealing communication scheme for RIS-empowered OFDM wireless systems. The proposed scheme is able to transmit data symbols avoiding any channel training stage, where neither reference signals nor the requirement for solving complex design optimization problems for both the BS and RIS parameters are needed. The proposed NCDS with the random RIS phase rotations enables the advantages offered by RISs with massive numbers of elements, as well as supporting medium/high mobility and/or low-SNR scenarios.

The proposed method was shown to be simple, yet effective, as compared to classical RIS-empowered systems based on CDS. In contrast to that conventional modulation scheme, the presented analysis of the SINR and SEP for both IID Rayleigh and a geometric wideband channel model revealed that, the NCDS-based performance is not only improved with increasing the number of BS antennas, but it can be strongly boosted when the number of the RIS unit elements is large. This trend was shown to be present irrespective of the possible low-phase resolution of RIS elements, which actually represent the majority of the available RIS hardware implementations. For future work, we intend to devise NCDS for RIS-empowered multiuser MISO OFDM communications and study optimized RIS phase configurations, in place of the random ones, with the goal to improve further the achievable performance, while avoiding time-consuming complex optimizations and communication of training symbols.

ACKNOWLEDGEMENT

This work has been funded by the Spanish National project IRENE-EARTH (PID2020-115323RB-C33 / AEI / 10.13039/501100011033) and the European EU H2020 RISE-6G project under grant number 101017011.

REFERENCES

[1] C. Huang, A. Zappone, G. C. Alexandropoulos, M. Debbah, and C. Yuen. "Reconfigurable Intelligent Surfaces for Energy Efficiency in Wireless Commu-

nication". In: *IEEE Trans. Wireless Commun.* 18.8 (Aug. 2019), pp. 4157–4170. ISSN: 1558-2248.

[2] M. Di Renzo, M. Debbah D.-T. Phan-Huy, A. Zappone, M.-S. Alouini, C. Yuen, V. Sciancalepore, G. C. Alexandropoulos, J. Hoydis, H. Gacanin, J. de Rosny, A. Bounceu, and G. Lerosey. "Smart radio environments empowered by reconfigurable AI meta-surfaces: an idea whose time has come". In: *EURASIP J. Wireless Commun. Net.* 2019.1 (May 2019), pp. 1–20.

[3] Q. Wu and R. Zhang. "Intelligent Reflecting Surface Enhanced Wireless Network via Joint Active and Passive Beamforming". In: *IEEE Trans. Wireless Commun.* 18.11 (Nov. 2019), pp. 5394–5409. ISSN: 1558-2248.

[4] C. Huang, S. Hu, G. C. Alexandropoulos, A. Zappone, C. Yuen, R. Zhang, M. D. Renzo, and M. Debbah. "Holographic MIMO Surfaces for 6G Wireless Networks: Opportunities, Challenges, and Trends". In: *IEEE Wireless Commun.* 27.5 (Oct. 2020), pp. 118–125. ISSN: 1558-0687.

[5] *NR; Physical channels and modulation (Release 17)*. Technical Report 38.211. France: 3GPP, 2022.

[6] *The Next Hyper-Connected Experience for All*. White Paper. Samsung 6G Vision, June 2020.

[7] *Study on channel model for frequencies from 0.5 to 100 GHz (Release 17)*. Technical Report 38.901. France: 3GPP, 2022.

[8] D. Serghiou, M. Khalily, T. W.C. Brown, and R.Tafazolli. "Terahertz Channel Propagation Phenomena, Measurement Techniques and Modeling for 6G Wireless Communication Applications: A Survey, Open Challenges and Future Research Directions". In: Jan. 2022, [Online] https://doi.org/10.36227/techrxiv.18092522.v2.

[9] G. C. Alexandropoulos, G. Lerosey, M. Debbah, and M. Fink. "Reconfigurable intelligent surfaces and metamaterials: The potential of wave propagation control for 6G wireless communications". In: *IEEE ComSoc TCCN Newslett.* 6.1 (June 2020), pp. 25–37.

[10] G. C. Alexandropoulos and E. Vlachos. "A hardware architecture for reconfigurable intelligent surfaces with minimal active elements for explicit channel estimation". In: *Proc. IEEE ICASSP*. Barcelona, Spain, May 2020, pp. 9175–9179.

[11] Z. Abu-Shaban, K. Keykhosravi, M. F. Keskin, G. C. Alexandropoulos, G. Seco-Granados, and H. Wymeersch. "Near-field localization with a reconfigurable intelligent surface acting as lens". In: *Proc. IEEE ICC*. Montreal, Canada, June 2021 [Online] arxiv.org/abs/2010.05617, pp. 1–6.

[12] N. Shlezinger, G. C. Alexandropoulos, M. F. Imani, Y. C. Eldar, and D. R. Smith. "Dynamic metasurface antennas for 6G extreme massive MIMO communications". In: *IEEE Wireless Commun.* 28.2 (Apr. 2021), pp. 106–113.

[13] M. Jian, G. C. Alexandropoulos, E. Basar, C. Huang, R. Liu, Y. Liu, and Chau Yuen. "Reconfigurable Intelligent Surfaces for Wireless Communications: Overview of Hardware Designs, Channel Models, and Estimation Techniques". In: *Intell. Converged Netw.* 2.2 (Dec. 2021), pp. 1–19.

[14] D. Mishra and H. Johansson. "Channel Estimation and Low-complexity Beamforming Design for Passive Intelligent Surface Assisted MISO Wireless Energy Transfer". In: *Proc. IEEE ICASSP*. Brighton, UK, May 2019, pp. 4659–4663.

[15] S. Lin, B. Zheng, G. C. Alexandropoulos, M. Wen, M. Di Renzo, and F. Chen. "Reconfigurable intelligent surfaces with reflection pattern modulation: Beamforming design, channel estimation, and achievable rate analysis". In: *IEEE Trans. Wireless Commun.* 20.2 (Feb. 2021), pp. 741–754.

[16] G. López-Lanuza, K. Chen-Hu, and A. G. Armada. "Deep Learning-Based Optimization for Reconfigurable Intelligent Surface-Assisted Communications". In: *Proc. IEEE WCNC*. Austin, USA, Apr. 2022.

[17] T. L. Jensen and E. De Carvalho. "An Optimal Channel Estimation Scheme for Intelligent Reflecting Surfaces Based on a Minimum Variance Unbiased Estimator". In: *Proc. IEEE ICASSP*. Barcelona, Spain, May 2020, pp. 5000–5004.

[18] Z. He and X. Yuan. "Cascaded Channel Estimation for Large Intelligent Metasurface Assisted Massive MIMO". In: *IEEE Wireless Commun. Lett.* 9.2 (Feb. 2020), pp. 210–214.

[19] H. Liu, X. Yuan, and Y. A. Zhang. "Matrix-Calibration-Based Cascaded Channel Estimation for Reconfigurable Intelligent Surface Assisted Multiuser MIMO". In: *IEEE J. Sel. Areas Commun.* 38.11 (Nov. 2020), pp. 2621–2636.

[20] C. You, B. Zheng, and R. Zhang. "Channel Estimation and Passive Beamforming for Intelligent Reflecting Surface: Discrete Phase Shift and Progressive Refinement". In: *IEEE J. Sel. Areas Commun.* 38.11 (Nov. 2020), pp. 2604–2620.

[21] Q. -U. -A. Nadeem, H. Alwazani, A. Kammoun, A. Chaaban, M. Debbah, and M. -S. Alouini. "Intelligent Reflecting Surface-Assisted Multi-User MISO Communication: Channel Estimation and Beamforming Design". In: *IEEE Open J. Commun. Society* 1 (May 2020), pp. 661–680.

[22] B. Zheng and R. Zhang. "Intelligent Reflecting Surface-Enhanced OFDM: Channel Estimation and Reflection Optimization". In: *IEEE Wireless Commun. Lett.* 9.4 (Apr. 2020), pp. 518–522.

[23] L. Wei, C. Huang, G. C. Alexandropoulos, and C. Yuen. "Parallel factor decomposition channel estimation in RIS-assisted multi-user MISO communication". In: *Proc. IEEE SAM*. Hangzhou, China, June 2020, pp. 1–6.

[24] Y. Yang, B. Zheng, S. Zhang, and R. Zhang. "Intelligent Reflecting Surface Meets OFDM: Protocol Design and Rate Maximization". In: *IEEE Trans. Wireless Commun.* 68.7 (July 2020), pp. 4522–4535.

[25] N. K. Kundu and M. R. McKay. "Large Intelligent Surfaces with Channel Estimation Overhead: Achievable Rate and Optimal Configuration". In: *IEEE Wireless Commun. Lett.* 10.5 (May 2021), pp. 986–990.

[26] T. Hwang, C. Yang, G. Wu, S. Li, and G. Y. Li. "OFDM and Its Wireless Applications: A Survey". In: *IEEE Trans. Veh. Technol.* 58.4 (May 2009), pp. 1673–1694.

[27] Jun Cai, Xuemin Shen, and J. W. Mark. "Robust channel estimation for OFDM wireless communication systems". In: *IEEE Trans. Wireless Commun.* 3.6 (Nov. 2004), pp. 2060–2071.

[28] C. Huang, G. C. Alexandropoulos, A. Zappone, M. Debbah, and C. Yuen. "Energy Efficient Multi-User MISO Communication Using Low Resolution Large Intelligent Surfaces". In: *Proc. IEEE GLOBECOM*. Abu Dhabi, UAE, Dec. 2018, pp. 1–6.

[29] C. You, B. Zheng, and R. Zhang. "Fast Beam Training for IRS-Assisted Multiuser Communications". In: *IEEE Wireless Commun. Lett.* 9.11 (Nov. 2020), pp. 1845–1849.

[30] V. Jamali, G. C. Alexandropoulos, R. Schober, and H. V. Poor. "Low-to-Zero-Overhead IRS Reconfiguration: Decoupling Illumination and Channel Estimation". In: *IEEE Commun. Lett.* 16.4 (Apr. 2022), pp. 932–936.

[31] G. C. Alexandropoulos, V. Jamali, R. Schober, and H. V. Poor. "Near-Field Hierarchical Beam Management for RIS-Enabled Millimeter Wave Multi-Antenna Systems". In: (2022, [Online] https://arxiv.org/abs/2203.15557.pdf).

[32] Constantinos Psomas, Ilias Chrysovergis, and Ioannis Krikidis. "Random Rotation-based Low-Complexity Schemes for Intelligent Reflecting Surfaces". In: *2020 IEEE PIMRC.* Aug. 2020, pp. 1–6.

[33] Qurrat-Ul-Ain Nadeem, Alessio Zappone, and Anas Chaaban. "Intelligent Reflecting Surface Enabled Random Rotations Scheme for the MISO Broadcast Channel". In: *IEEE Tran. on Wireless Commun.* (2021), Early Access. ISSN: 1558-2248.

[34] R. A. Smith. "The relative advantages of coherent and incoherent detectors: a study of their output noise spectra under various conditions". In: *Proceedings of the IEE - Part III: Radio and Commun. Eng.* 98.55 (Sept. 1951), pp. 401–406.

[35] D. Middleton. "Statistical theory of signal detection". In: *Transactions of the IRE Professional Group on Info. Theory* 3.3 (Mar. 1954), pp. 26–51. ISSN: 2168-2704.

[36] M. L. Doelz, E. T. Heald, and D. L. Martin. "Binary Data Transmission Techniques for Linear Systems". In: *Proceedings of the IRE* 45.5 (May 1957), pp. 656–661. ISSN: 2162-6634.

[37] A. Manolakos, M. Chowdhury, and A. J. Goldsmith. "CSI is not needed for optimal scaling in multiuser massive SIMO systems". In: *2014 IEEE ISIT*. June 2014, pp. 3117–3121.

[38] M. Chowdhury, A. Manolakos, and A. Goldsmith. "Scaling Laws for Noncoherent Energy-Based Communications in the SIMO MAC". In: *IEEE Trans. Info. Theory* 62.4 (Apr. 2016), pp. 1980–1992. ISSN: 1557-9654.

[39] A. G. Armada and L. Hanzo. "A non-coherent multiuser large scale SIMO system relaying on M-ary DPSK". In: *Proc. IEEE ICC*. June 2015, pp. 2517–2522.

[40] K. Chen-Hu and A. G. Armada. "Non-Coherent Multiuser Massive MIMO-OFDM with Differential Modulation". In: *Proc. IEEE ICC*. May 2019, pp. 1–6.

[41] K. Chen-Hu, Y. Liu, and A. G. Armada. "Non-Coherent Massive MIMO-OFDM Down-Link Based on Differential Modulation". In: *IEEE Trans. Veh. Technol.* 69.10 (Oct. 2020), pp. 11281–11294. ISSN: 1939-9359.

[42] K. Chen-Hu, Y. Liu, and A. G. Armada. "Non-coherent massive MIMO-OFDM for communications in high mobility scenarios". In: *ITU J. Future and Evolving Technol.* 1.1 (Dec. 2020), pp. 13–24.

[43] M. J. Lopez-Morales, K. Chen-Hu, and A. Garcia-Armada. "Differential Data-Aided Channel Estimation for Up-Link Massive SIMO-OFDM". In: *IEEE Open J. of the Commun. Society* 1 (July 2020), pp. 976–989. ISSN: 2644-125X.

[44] F. Adachi. "Adaptive differential detection for M-ary DPSK". In: *IEEE Proceedings - Communications* 143.1 (Feb. 1996), pp. 21–28. ISSN: 1350-2425.

[45] M. Shafi, J. Zhang, H. Tataria, A. F. Molisch, S. Sun, T. S. Rappaport, F. Tufvesson, S. Wu, and K. Kitao. "Microwave vs. Millimeter-Wave Propagation Channels: Key Differences and Impact on 5G Cellular Systems". In: *IEEE Commun. Mag.* 56.12 (Dec. 2018), pp. 14–20. ISSN: 1558-1896.

[46] C. Gustafson, K. Haneda, S. Wyne, and F. Tufvesson. "On mm-Wave Multipath Clustering and Channel Modeling". In: *IEEE Trans. Antennas and Propagation* 62.3 (Mar. 2014), pp. 1445–1455. ISSN: 1558-2221.

[47] M. R. Akdeniz, Y. Liu, M. K. Samimi, S. Sun, S. Rangan, T. S. Rappaport, and E. Erkip. "Millimeter Wave Channel Modeling and Cellular Capacity Evaluation". In: *IEEE J. Sel. Areas in Commun.* 32.6 (June 2014), pp. 1164–1179. ISSN: 1558-0008.

[48] Chao Wang, Zan Li, Jia Shi, and Derrick Wing Kwan Ng. "Intelligent Reflecting Surface-Assisted Multi-Antenna Covert Communications: Joint Active and Passive Beamforming Optimization". In: *IEEE Trans. on Commun.* (2021), Early Access. ISSN: 1558-0857.

[49] Ibrahim Yildirim, Ali Uyrus, and Ertugrul Basar. "Modeling and Analysis of Reconfigurable Intelligent Surfaces for Indoor and Outdoor Applications in Future Wireless Networks". In: *IEEE Trans. on Commun.* 69.2 (Feb. 2021), pp. 1290–1301. ISSN: 1558-0857.

[50] Saman Atapattu, Rongfei Fan, Prathapasinghe Dharmawansa, Gongpu Wang, Jamie Evans, and Theodoros A. Tsiftsis. "Reconfigurable Intelligent Surface Assisted Two–Way Communications: Performance Analysis and Optimization". In: *IEEE Trans. on Commun.* 68.10 (Oct. 2020), pp. 6552–6567. ISSN: 1558-0857.

[51] George Arfken. *Mathematical Methods for Physicists*. Third. San Diego: Academic Press, Inc., 1985.

[52] K. Chen-Hu, G. C. Alexandropoulos, and A. G. Armada. "Non-Coherent MIMO-OFDM Uplink empowered by the Spatial Diversity in Reflecting Surfaces". In: *Proc. IEEE WCNC*. Austin, USA, Apr. 2022.

[53] G. C. Alexandropoulos, K. Katsanos, M. Wen, and D. B. da Costa. "Safeguarding MIMO Communications with Reconfigurable Metasurfaces and Artificial Noise". In: *Proc. IEEE ICC*. Montreal, Canada, June 2021, [Online] arxiv.org/abs/2005.10062.

[54] M. M. Zhao, Q. Wu, M. J. Zhao, and R. Zhang. "Intelligent Reflecting Surface Enhanced Wireless Networks: Two-Timescale Beamforming Optimization". In: *IEEE Trans. Wireless Commun.* 20.1 (Jan. 2021), pp. 2–17. ISSN: 1558-2248.

AUTHORS

Kun Chen-Hu received his Ph.D. degree in multimedia and communications in 2019 from Universidad Carlos III de Madrid (Spain). Currently, he is a postdoctoral researcher in the same institution. He was awarded by UC3M in 2019 recognizing his outstanding professional career after graduation. He visited Eurecom (France) and Vodafone Chair TU Dresden (Germany), both as guest researcher. He also participated in different research projects in collaboration with several top companies in the area of mobile communications. He is the Web Chair for Globecom 2021, Madrid (Spain), and online content editor for IEEE ComSoc. His research interests are related to signal processing techniques, such as waveforms design, reconfigurable intelligent surfaces, non-coherent massive MIMO and channel estimation.

George C. Alexandropoulos received an engineering diploma, M.A.Sc., and Ph.D. degrees in computer engineering and informatics from the the School of Engineering, University of Patras, Greece in 2003, 2005, and 2010, respectively. He has held research positions at various Greek universities and research institutes, as well as at the Mathematical and Algorithmic Sciences Lab, Paris Research Center, Huawei Technologies France, and he is currently an assistant professor with the Department of Informatics and Telecommunications, School of Sciences, National and Kapodistrian University of Athens (NKUA), Greece. He also serves as a principal researcher at the Technology Innovation Institute, Abu Dhabi, United Arab Emirates. He currently serves as an editor for IEEE Transactions on Communications, IEEE Wireless Communications Letters, ELSEVIER Computer Networks, Frontiers in Communications and Networks, and the ITU Journal on Future and Evolving Technologies. In the past, he has held various fixed-term and guest editorial positions for IEEE Transactions on Wireless Communications and IEEE Communications Letters, as well as for various special issues at IEEE journals. Prof. Alexandropoulos is a Senior Member of the IEEE Communications, Signal Processing, and Information Theory Societies as well as a registered Professional Engineer of the Technical Chamber of Greece. He is also a Distinguished Lecturer of the IEEE Communications Society. He has participated and/or technically managed more than 10 European Union (EU) research and innovation projects, as well as several Greek and international research projects. He is currently NKUA's principal investigator for the EU H2020 RISE-6G research and innovation project dealing with RIS-empowered smart wireless environments. He has received the best Ph.D. thesis award 2010, the IEEE Communications Society Best Young Professional in Industry Award 2018, the EURASIP Best Paper Award of the Journal on Wireless Communications and Networking 2021, the IEEE Marconi Prize Paper Award in Wireless Communications 2021, and a Best Paper Award from the IEEE GLOBECOM 2021. His research interests span the general areas of algorithmic design and performance analysis for wireless networks with emphasis on multi-antenna transceiver hardware architectures, active and passive reconfigurable metasurfaces, integrated communications and sensing, millimeter

wave and THz communications, as well as distributed machine learning algorithms. More information is available at www.alexandropoulos.info.

Ana García Armada received a Ph.D. degree in electrical engineering from the Polytechnical University of Madrid in February 1998. She is currently a professor at Universidad Carlos III de Madrid, Spain. She is leading the Communications Research Group at this university. She has participated in more than 30 national and 10 international research projects as well as 20 contracts with the industry. Her research has resulted in 9 book chapters, and more than 150 publications in prestigious international journals and conferences, as well as 5 patents. She has also contributed to standardization organizations (ITU, ETSI) and is a member of the European 5G PPP Group of Experts, as well as the Spanish representative on the committee of the ESA Joint Board on Communication Satellite Programs 5G Advisory Committee (5JAC). She has been editor (2016–2019, Exemplary Editor Award 2017 and 2018) and area editor (2019-2020, Exemplary Editor Award 2020) of IEEE Communication Letters. She is the editor of IEEE Transactions on Communications since 2019, area editor of IEEE Open Journal of the Communications Society since 2019, editor of the ITU Journal on Future and Evolving Technologies and is a regular member of the technical program committees of the most relevant international conferences in their field. She has formed / is part of the organizing committee of the IEEE Globecom 2019 and 2021 (General Chair), IEEE Vehicular Technology Conference Spring 2018, 2019 and Fall 2018, IEEE 5G Summit 2017, among others. She is Secretary of the IEEE ComSoc Signal Processing and Computing for Communications Committee, has been Secretary and Chair of the IEEE ComSoc Women in Communications Engineering Standing Committee. Since January 2020 she is Director of Online Content of the IEEE Communications So- ciety. She has received the Award of Excellence from the Social Council and the Award for Best Teaching Practices from Universidad Carlos II de Madrid, as well as the third place Bell Labs Prize 2014, the Outstanding Service Award 2019 from the SPCE committee of the IEEE Communications Society and the Outstanding Service Award 2020 from the Women in Communications Engineering (WICE) standing committee.